THE JOURNAL OF PHYSICAL CHEMISTRY A

Article

pubs.acs.org/JPCA

N−H Stretching Excitations in Adenosine-Thymidine Base Pairs in Solution: Pair Geometries, Infrared Line Shapes, and Ultrafast Vibrational Dynamics

Christian Greve,[†] Nicholas K. Preketes,[‡] Henk Fidder,[†] Rene Costard,[†] Benjamin Koeppe,[†] Ismael A. Heisler,[†] Shaul Mukamel,[‡] Friedrich Temps,[§] Erik T. J. Nibbering,*[,†] and Thomas Elsaesser[†]

[†]Max Born Institut für Nichtlineare Optik und Kurzzeitspektroskopie, Max Born Strasse 2A, D-12489 Berlin, Germany

[‡]Department of Chemistry, University of California, Irvine, California 92697-2025, United States

[§]Institut für Physikalische Chemie, Christian-Albrechts-Universität zu Kiel, Olshausenstrasse 40, D-24098 Kiel, Germany

Supporting Information

ABSTRACT: We explore the N−H stretching vibrations of adenosine-thymidine base pairs in chloroform solution with linear and nonlinear infrared spectroscopy. Based on estimates from NMR measurements and ab initio calculations, we conclude that adenosine and thymidine form hydrogen bonded base pairs in Watson−Crick, reverse Watson−Crick, Hoogsteen, and reverse Hoogsteen configurations with similar probability. Steady-state concentration and temperature dependent linear FT-IR studies, including H/D exchange experiments, reveal that these hydrogen-bonded base pairs have complex N−H/N−D stretching spectra with a multitude of spectral components. Nonlinear 2D-IR spectroscopic results, together with IR-pump-IR-probe measurements, as also corroborated by ab initio calculations, reveal that the number of N−H stretching transitions is larger than the total number of N−H stretching modes. This is explained by couplings to other modes, such as an underdamped low-frequency hydrogen-bond mode, and a Fermi resonance with NH_2 bending overtone levels of the adenosine amino-group. Our results demonstrate that modeling based on local N−H stretching vibrations only is not sufficient and call for further refinement of the description of the N−H stretching manifolds of nucleic acid base pairs of adenosine and thymidine, incorporating a multitude of couplings with fingerprint and low-frequency modes.

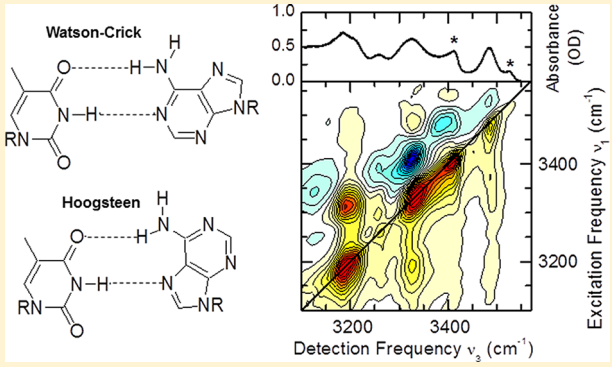

1. INTRODUCTION

Nucleobase pairing enables the encoding of genetic information in DNA and RNA. Nucleobase pairing occurs through particular hydrogen bonding geometries of complementary bases, i.e., between guanine (G) and cytosine (C) or between adenine (A) and thymine (T) or uracil (U). Different base pair geometries such as Watson−Crick, wobble, or Hoogsteen configurations appear depending on the structure and steric constraints of the molecular environment. X-ray and neutron diffraction of crystalline DNA or RNA, and also solid crystals of the nucleic acid bases themselves, have shed light onto the pairing geometries and the hydrogen bond strength in the nucleobase pairs.[1,2] This structural information has been compared to quantum chemical calculations.[3−7]

An alternative approach that provides insight into the hydrogen bonding between nucleobases is linear vibrational spectroscopy, which has mainly focused on the stretching vibrations of the hydrogen donating N−H groups. As a hallmark of hydrogen bonding, the red-shift of the N−H stretching frequency compared to that of a free N−H group has been analyzed in some detail. This information has been correlated with structural information obtained with NMR[8,9] or IR spectroscopy.[6,10,11] The resulting semiempirical plots connect a particular nuclear spin chemical resonance shift or a vibrational frequency shift to a particular value of the hydrogen bond strength. One should realize, however, that these correlation plots have been obtained by accumulating data on many different types of structures, ensemble averaged in time and in chemical surroundings. As such it remains for every hydrogen-bonded complex an open issue to which degree reliable structural information can be obtained from this type of analysis.

Beyond its role in defining structure, hydrogen bonding of nucleobase pairs has a strong influence on molecular, in particular vibrational couplings between different functional groups and, moreover, on vibrational decoherence, population lifetimes, and relaxation pathways. Such dynamics occur in the femto- to picosecond time range. Both molecular couplings and vibrational dynamics modify the line shapes of vibrational bands substantially, a fact that has mainly been neglected in

Received: October 15, 2012
Revised: December 6, 2012
Published: December 12, 2012

deriving empirical relations between frequency shifts and hydrogen bond geometries. Ultrafast nonlinear infrared (IR) spectroscopy has given insight into molecular couplings and the resulting nonequilibrium dynamics. This information has also allowed for analyzing complex vibrational line shapes in a number of model systems.[12−19]

In the present work, we present an experimental and theoretical study of the base pairing of adenosine and thymidine in liquid solution, combining NMR, linear, and ultrafast nonlinear IR spectroscopy with ab initio theoretical calculations of ground state energies, vibrational frequencies, and anharmonic couplings. Chemically modified 2′-deoxyadenosine and 2′-deoxythymidine nucleosides are studied in chloroform solution. As opposed to DNA duplex geometries, or chemically modified A·U[20] and G·C base pairs,[21] that all have Watson−Crick (WC) geometries, hydrogen bonding between A and T nucleosides in chloroform can lead to Watson−Crick (WC) and reverse Watson−Crick (rWC) or Hoogsteen (H) and reverse Hoogsteen (rH) pairing (see Figure 1), akin to hydrogen bonding geometries found in gas

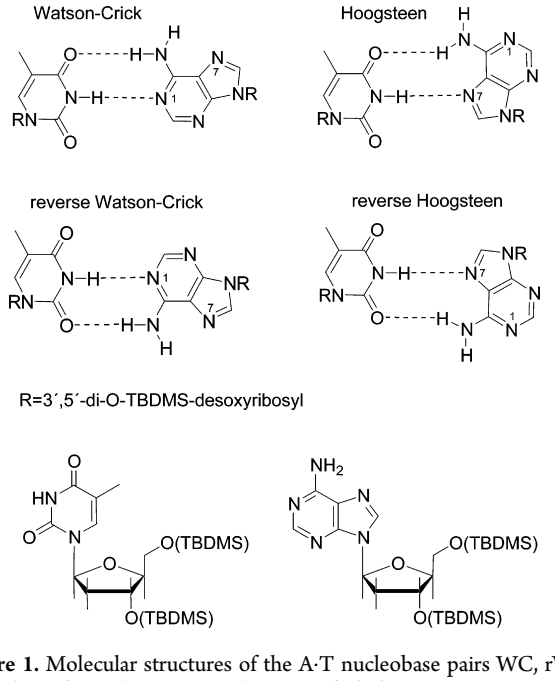

Figure 1. Molecular structures of the A·T nucleobase pairs WC, rWC, H, and rH, formed upon complexation of 3′,5′-TBDMS protected 2′-deoxyadenosine and 3′,5′-TBDMS protected 2′-deoxythymidine (with TBDMS standing for tert-butyldimethylsilyl) as shown in the bottom of the graph.

phase studies.[6,22,23] We first analyze the relative abundance of such species with NMR measurements and theoretical estimates. This information serves as an input for studying vibrational spectra, couplings, and dynamics of the A·T pairs.

The outline of the paper is as follows. After describing our experimental and theoretical methods in section 2, we summarize the results of the NMR study and theoretical ground state energies in section 3. In section 4, we explore steady-state concentration and temperature-dependent FT-IR spectra to determine whether distinct N−H stretching marker modes exist for particular base pairs. By a comparison of the N−H and N−D stretching manifolds by use of H/D exchange and a comparison with theoretically calculated vibrational frequencies and transition strengths for different nucleobase pairing geometries we show the intricacies of making assignments based on linear FT-IR spectra only. In section 5, we then present results from femtosecond IR pump−probe and 2D measurements on A·T base pairs, giving direct evidence of the pronounced couplings between different N−H stretching excitations and providing insight into vibrational dynamics. We show that the picture of localized stretching modes of the two hydrogen bonded N−H groups in the complexes breaks down and has to be replaced by a description in terms of strongly coupled modes. Conclusions are given in section 6.

2. METHODS

Chemical Synthesis. To warrant a sufficient A·T base pairing in Watson−Crick or Hoogsteen-type geometries without complications of tautomerization, we have synthesized chemically modified 2′-deoxyadenosine and 2′-deoxythymidine nucleosides in a similar fashion as reported before.[24] To increase the solubilities in weakly polar solvents, the hydroxyl groups of the ribose units were substituted with tert-butyldimethylsilyl (TBDMS) groups. For our purposes we denote these chemically modified nucleic bases 3′,5′-TBDMS protected 2′-deoxyadenosine and 3′,5′-TBDMS protected 2′-deoxythymidine as A and T, respectively. Solutions of nucleosides partially deuterated in the mobile proton sites were obtained in the following fashion. Substances were dissolved in a 100-fold excess amount of methanol-d_1, and after a few minutes, the solvent was removed in vacuum. After repetition of this procedure residues were taken up in chloroform resulting in solutions with a (70−80)% degree of nucleoside deuteration as estimated by FT-IR and ^{1}H NMR. Correspondingly, a single treatment with a 2:1 mixture of methanol-d_1 and methanol leads to about 50% deuteration.

NMR Measurements. NMR sample solutions in a Freon solvent mixture ($CDClF_2$ and CDF_3) were prepared by weighing solutes in sample tubes equipped with J. Young valves and subsequent addition of the solvent by vacuum transfer. Spectra were calibrated to 7.18 ppm for the residual solvent signal of $CHClF_2$. NMR samples in dichloromethane solution were prepared from 25 mM stock solutions; spectra were calibrated to 5.32 ppm for $CHDCl_2$.

Steady-State IR Measurements. FT-IR spectra were recorded with a Varian 640 FT-IR spectrometer (resolution 1 cm^{-1}) equipped with a Specac variable temperature unit. For the linear IR measurements our solutions were held between 1 mm CaF_2 windows with absorption path lengths of 0.2 or 1 mm using Teflon spacers. The solvents were dried over molecular sieves with pore diameters of 0.3 nm.

Ultrafast IR Measurements. We have performed femtosecond mid-IR pump−probe and three pulse 2D-IR photon echo experiments as described before.[21] In short, for the 2D-IR experiments the mid-IR pulses were generated by parametric downconversion of the output of a 1 kHz regeneratively amplified Ti:sapphire laser system providing pulses with a center frequency of 3350 cm^{-1} and 50 fs pulse duration. Two pairs of passively phase-locked pulses with a pulse energy of 500 nJ each were generated by a diffractive optics setup, and one of those pulses was attenuated by 99% to serve as a local oscillator for spectral interferometric detection of the generated nonlinear signal. The 2D-IR spectra have a resolution of 4 cm^{-1} along the excitation frequency ν_1 and 9 cm^{-1} along the detection frequency ν_3.

The same setup was used for one-color pump−probe experiments with two of the four pulses blocked, while the

dx.doi.org/10.1021/jp310177e | J. Phys. Chem. A 2013, 117, 594−606

attenuated probe pulse was detected in a spectrally resolved way to monitor pump-induced absorbance changes in the sample. In contrast, two-color transient absorption measurements were performed with an amplified 1 kHz Ti:sapphire laser system seeding two parametric frequency converters that deliver independently tunable pump and probe pulses with pulse energies of typically 2 μJ and pulse durations of about 100 fs.

For the ultrafast experiments we used A·T sample solutions prepared by mixing identical volumes of a 240 mM solution of A with a 240 mM solution of T yielding a 120 mM solution of A·T. These solutions were held between 1 mm CaF_2 windows with absorption path lengths of 0.2 mm, resulting in a peak IR absorbance of 0.6 at 3200 cm^{-1}.

Quantum Chemical Calculations. All calculations were performed using the Gaussian 09 software package.[25] Ab initio anharmonic frequency calculations were performed on the 9-methyladenine/1-methylthymine base pair (abbreviated as 9-mA·1-mT) in the gas-phase at the HF/6-311++G** level of theory. The Hamiltonian and other details of the calculations are presented in section 4.2, together with the main results. Calculations of the relative energetics of the 3′,5′-TBDMS protected A·T base pair (Figure 1) were performed at the HF/6-311++G** level. For these calculations, the complete structure consisting of the nucleobase and ribose with TBDMS side groups were used, with the silicon atoms in the TBDMS groups replaced by carbon atoms. The polarizable continuum model with a conductor-like solvation model was used to perform the self-consistent reaction field calculations to simulate the presence of the chloroform solvent.[26,27]

3. EQUILIBRIUM STRUCTURES OF A·T BASE PAIRS IN SOLUTION

Low temperature ^{1}H NMR measurements of hydrogen bonded molecular systems in Freon solvents, where chemical exchange phenomena are substantially slowed down, have been shown to provide key insight into a significant number of hydrogen bonding geometries.[28−31] This approach is followed for the A·T base pairs, similar to previous work on the A·U base pair formation of 2′-deoxyadenosine and 2′-deoxyuridine derivatives.[8,9,32] We note here that ^{1}H chemical shifts of the imino protons in N-H···N are measured, in contrast to a study of ^{13}C chemical shifts,[33] where it has been realized[34] that such results are too small and too insensitive to correctly probe hydrogen bonds. In our studies the protons in the hydrogen bonds are measured, providing direct access to the hydrogen bond structure. While detailed results of the NMR measurements are given in the Supporting Information, we summarize the main conclusions as follows. At 140 K two signals are observed that can be attributed to the bridging protons in the N−H···N hydrogen bonds to N1 and N7 of A, i.e. WC/rWC and H/rH type of complexes. The chemical shifts measured for the A·T pairs are similar to those measured for A·U complexes under the same experimental conditions. This finding suggests similar geometries of the N−H···N hydrogen bonds in A·T and A·U complexes with N−H···N distances of about 2.9−3.0 Å.

Isomeric ratios of Watson−Crick and Hoogsteen complexes may be estimated from the experimentally determined signal ratios and derived free energy differences given in Table S1 of the Supporting Information. The free energy differences between Watson−Crick and Hoogsteen complexes are between 0.5 and 0.9 kJ mol^{-1}, i.e., substantially smaller than kT at 300 K (2.51 kJ mol^{-1}). This suggests that both types of complexes are present in significant amounts in the $CHCl_3$ solutions at room temperature.

The relative energetics of the TBDMS Hoogsteen and Watson−Crick complexes in chloroform were calculated using the polarizable continuum model with a conductor-like solvation model.[26,27] A recent density functional calculation of the relative energetics of alkyl substituted base-pairing conformations has suggested that the Hoogsteen type conformations are more stable than the Watson−Crick type conformations in the gas phase, while the Watson−Crick type conformations are more stable in chloroform.[7] Our calculations of the Born−Oppenheimer energies of the A·T complexes in chloroform indicate that the Watson−Crick complex is more stable than the Hoogsteen complex by 0.34 kJ mol^{-1} which is less than kT at 300 K. Our results agree with the difference in the free energies of association calculated at the SM8AD/M06−2x/6-31G** level (0.33 kJ mol^{-1}).[7]

Combining the results of the low temperature NMR measurements and the calculated Born−Oppenheimer energies, we conclude that all four A·T nucleobase pairs can be expected to be present in similar amounts in chloroform solution at room temperature. This finding has major repercussions for any interpretation of results from linear and nonlinear IR spectroscopy.

4. LINEAR N−H STRETCHING ABSORPTION OF A·T BASE PAIRS

4.1. Concentration- and Temperature-Dependent IR Spectra. Figure 2 shows the linear FT-IR spectra measured for solutions of T, A, and A·T in $CHCl_3/CDCl_3$. For the T

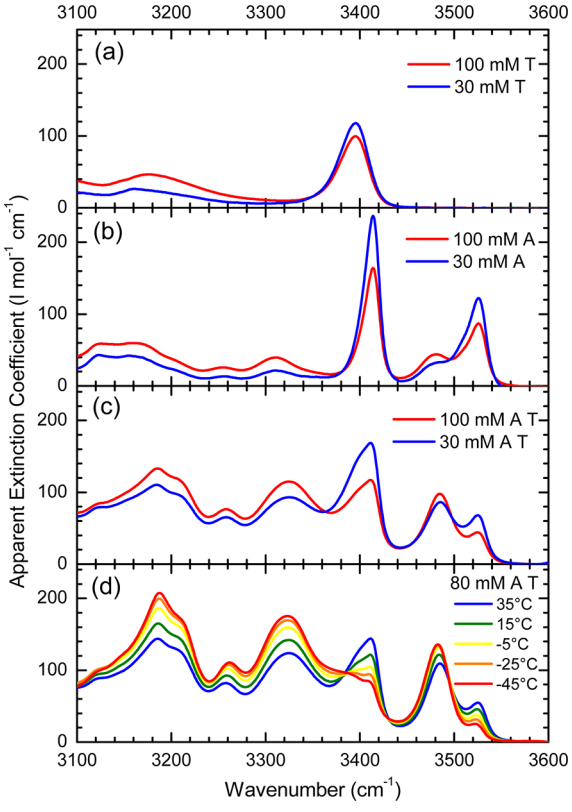

Figure 2. Solvent-corrected FT-IR spectra of (a) T, (b) A, and (c) A and T in equimolar amounts in $CDCl_3$, as well as of 80 mM A·T as function of temperature (d) in $CHCl_3$.

dx.doi.org/10.1021/jp310177e | J. Phys. Chem. A 2013, 117, 594−606

monomer the N−H stretching transition is located at 3396 cm^{-1} (Figure 2a). Upon increasing the concentration of T, the relative magnitude of this band decreases, and broader frequency downshifted bands appear at 3176 and 3068 cm^{-1}. The latter two bands suggest the formation of T·T complexes with different hydrogen bond geometries in $CHCl_3$ solution, in accordance with previously reported observations for complexes of 1-cyclohexyluracil in $CDCl_3$.[35] For the A monomer we observe two bands located at 3413 cm^{-1} and at 3525 cm^{-1} (Figure 2b), assigned to the symmetric and antisymmetric NH_2 stretching modes, respectively. At higher concentrations of A, bands indicative of A·A complexes appear at 3126, 3167, 3255, 3311, and 3482 cm^{-1}, in a similar fashion as observed for 9-ethyladenine and N-methyladenine in $CDCl_3$.[36] From the previously reported studies as well as those performed on cytidine derivatives[37,38] we conclude that, besides dimers with different geometries, larger trimers or even tetramers may have significant relative concentrations under the conditions used to record these spectra.

A significantly different band pattern arises when A and T are dissolved in $CHCl_3$ in equimolar amounts (Figure 2c). We observe distinct spectral features at 3188, 3211, 3262, and 3324 cm^{-1} that can clearly be ascribed to A·T complexes, as these are absent in the spectra of A·A or T·T. The peak positions are similar to those observed for complexes of adenine and uracil derivatives in solution.[20,39,40] Moreover, the narrow 3484 cm^{-1} band is due to the A·T base pairs, as well as A·A complexes. In addition, one observes the N−H stretching bands of A and T monomers. A small shoulder at 3126 cm^{-1} may also be a signature of A·A complexes. The N−H stretching manifold of A·T becomes more pronounced upon lowering the temperature of the sample (Figure 2d; cf. a measurement on A·T in CH_2Cl_2 at even lower temperatures is shown in Figure S2, Supporting Information).

Figure 3a shows the comparison of the linear IR spectra of T, A, and A·T on an extended scale, now also including the range of CH stretching absorption between 2800 and 3000 cm^{-1} and the region below. Close inspection reveals that besides the multiple number of N−H stretching features for A·T complexes observed in the 3100−3500 cm^{-1} region, a distinct wing extends from the C−H stretch region down to 2400 cm^{-1}. For T·T and A·A complexes this low-frequency wing appears to be smaller in magnitude under working concentrations. In the A·T case, the absorption wing represents a major absorption feature with a similar strength as the N−H stretching features located at 3188 and 3324 cm^{-1}.

H/D exchange was performed for A, T, and A·T to obtain additional insight into the N−H stretching band pattern. Figure 3b shows that with a fractional H/D-exchange the N−H stretching components as observed in Figures 2c,d and 3a decrease in magnitude, while new N−D stretching features appear at lower frequencies. The narrow bands observed at 2488, 2565, 2604, and 2639 cm^{-1} indicate free N−D stretching modes. The broader frequency-downshifted band at 2419 cm^{-1}, as well as the broad feature with several maxima centered at 2170 cm^{-1}, are related to hydrogen-bonded N−D stretching modes. The low-frequency wing of this 2170 cm^{-1} band corresponds to the tail between 2400 and 3000 cm^{-1} observed in the A·T spectrum of Figure 3a. In the spectrum of the partially deuterated sample (Figure 3b), a new band shows up at 3469 cm^{-1}, i.e., halfway between the symmetric and asymmetric stretching modes of A. This band is due to the N−H stretching mode of A monomers with an NHD-group.[41]

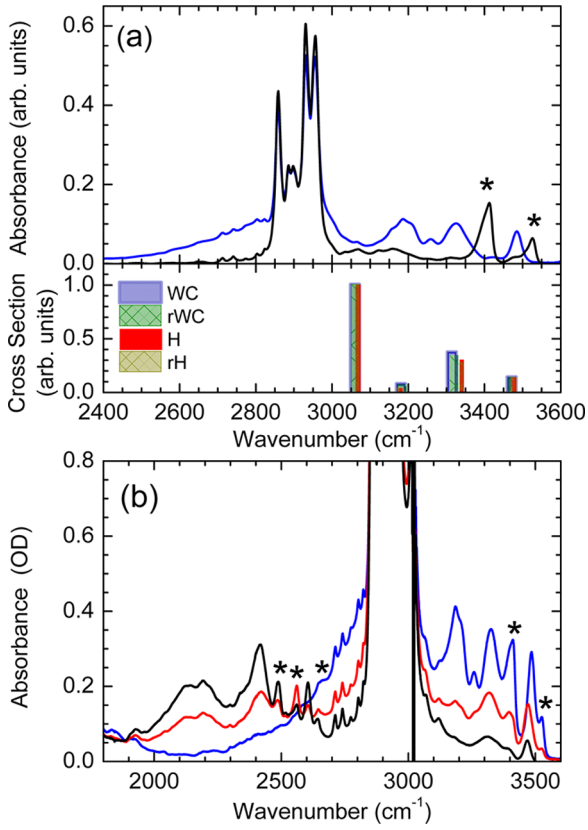

Figure 3. (a) Comparison of FT-IR spectra of solutions of A or T only and of A·T in $CDCl_3$ solution. The sum of A and T monomer spectra is shown as the black curve, whereas the A·T spectrum (blue line) has been obtained after subtraction of monomer peaks. For comparison underneath the calculated transitions of the four different nucleobase pairs are shown as stick spectra. (b) Results of the H/D exchange experiment, for different degrees of deuteration: 0% (blue line), 50% (red line), 85% (black line). In these spectra monomer peaks are indicated with asterisks. In both panels the band assignment in local mode representation follows from our findings in the linear FT-IR and nonlinear 2D-IR spectra.

4.2. Theoretical Calculations of N−H Stretching Spectra. Ab initio calculations were performed to analyze the frequency positions of the different N−H stretching bands and to get insight into anharmonic couplings between the different modes. We have chosen to use the HF/6-311++G** level of theory. From normal mode calculations using various exchange-correlation procedures with the SV(P) basis set[42] (Table S2, Supporting Information), we found that DFT methods underestimate the frequency of the thymine N−H stretch. This causes the thymine N−H stretch to have a lower frequency than the C−H stretching band. This deviation may be due to an overestimation of the hydrogen bond strength for the thymine N−H group, as all DFT methods predict shorter N−H bond distances when compared to the HF/SV(P) calculations (Table S2, Supporting Information). The HF/6-311++G** potential energy surface of the 9-mA·1-mT complexes was expanded to sixth order in the three N−H stretching and the NH_2 bending internal coordinates:[43−45]

$$H = H_0 + H_1 \quad (1a)$$

dx.doi.org/10.1021/jp310177e | J. Phys. Chem. A 2013, 117, 594−606

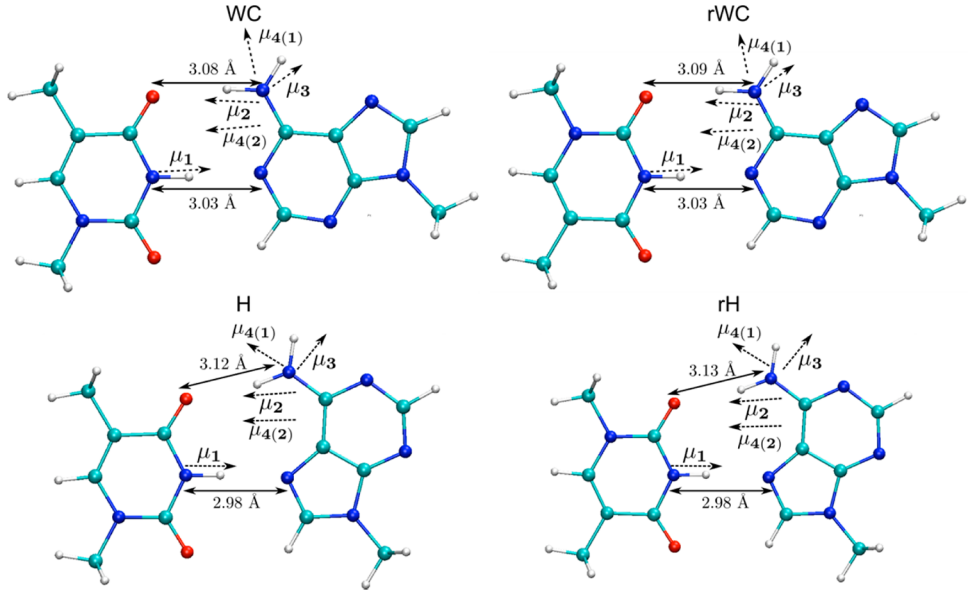

Figure 4. A·T base pair geometries of the WC, rWC, H, and rH obtained with ab initio calculations, as well as orientations of transition dipole moments μ_i (i = 1, 2, 3) of the fundamental N−H stretching transitions and μ_i (i = 4(1), 4(2)) of the fundamental and first overtone transitions of the NH_2 bending mode, as specified in Table 3. For details see text.

$$H_0 = V_0 + \sum_{i=1}^{3} f_i r_i + \frac{1}{2}\sum_{ij=1}^{3} G_{ij} p_i p_j + \frac{1}{2}\sum_{ij=1}^{3} f_{ij} r_i r_j + \frac{1}{3!}\sum_{ijk=1}^{3} f_{ijk} r_i r_j r_k + \frac{1}{4!}\sum_{ijkl=1}^{3} f_{ijkl} r_i r_j r_k r_l + \frac{1}{5!}\sum_{ijklm=1}^{3} f_{ijklm} r_i r_j r_k r_l r_m + \frac{1}{6!}\sum_{ijklmn=1}^{3} f_{ijklmn} r_i r_j r_k r_l r_m r_n \quad (1b)$$

$$H_1 = V_1 + f_4 r_4 + \frac{1}{2}\sum_{i=1}^{4} G_{i4} p_i p_4 + \frac{1}{2}\sum_{i=1}^{4} f_{i4} r_i r_4 + \frac{1}{3!}\sum_{i=1}^{3}\left(\frac{\partial G_{i4}}{\partial r_4}\right) p_i p_4 r_4 + \frac{1}{3!}\sum_{i=1}^{3}\left(\frac{\partial G_{44}}{\partial r_i}\right) r_i p_4^2 + \frac{1}{3!}\sum_{i=1}^{4} f_{i44} r_i r_4^2 + \frac{1}{4!} f_{4444} r_4^4 + \frac{1}{5!} f_{44444} r_4^5 + \frac{1}{6!} f_{44444} r_4^6 \quad (1c)$$

where r_i and p_i are the position and momentum of coordinate i, G_{ij} are elements of the Wilson G-Matrix,[46] and $f^{(n)}_{k1k2\cdots kn}$ are the nth order force constants:

$$f^{(n)}_{k1k2\cdots kn} = \left(\frac{\partial^n V}{\partial r_{k1}\partial r_{k2}\cdots\partial r_{kn}}\right)_0 \quad (2)$$

In eq 1, the thymine N−H stretching, hydrogen-bonded adenine N−H stretching, free adenine N−H stretching, and the NH_2 bending coordinates are represented by the indices 1, 2, 3, and 4, respectively. We will use this notation for the remainder of the manuscript. It should be noted that we only consider four internal coordinates in the current calculations as the size of the basis set grows exponentially with the number of modes included. The inclusion of coupling to other (harmonic) modes can be achieved using procedures such as VSCF[47,48] and VPT2[49] where the explicit diagonalization of the Hamiltonian is not necessary.

The Hamiltonian is written as a sum of two parts, $H = H_0 + H_1$, where H_0 contains terms with only the N−H stretching coordinates and H_1 contains terms related to the NH_2 bending and its coupling with the stretching coordinates. The nuclear dipole moment was truncated at first order:

$$\mu = \mu_0 + \sum_i \left(\frac{\partial \mu}{\partial r_i}\right)_0 r_i \quad (3)$$

The equilibrium force constants and transition dipole moments were determined by least-squares fits to the computed potential energy surface and electric dipole, respectively. The optimized geometries, which are planar (see Figure 4), agree with previous results.[5] The hydrogen bond lengths, which are in good agreement with experiment,[1,50,51] are also indicated in Figure 4. The potential energy surface and the electric dipole moment were calculated for displacements from equilibrium ranging from −0.2 to 0.2 Å in steps of 0.05 Å for the N−H stretching coordinates and from −20° to 20° in steps of 5° for the NH_2 bending coordinate.

Equation 1 can be rewritten in an equivalent form by transforming the coordinates using

$$r_i = \sqrt{\frac{\hbar G_{ii}}{2\omega_i}}\left(B_i + B_i^\dagger\right) \quad (4a)$$

$$p_i = i\sqrt{\frac{\hbar \omega_i}{2G_{ii}}}\left(B_i^\dagger - B_i\right) \quad (4b)$$

Here, B_i and $B_i^\dagger$ are the bosonic annihilation and creation operators which satisfy the commutation relation $[B_i, B_j^\dagger] = \delta_{ij}$. The Hamiltonian can now be written as

$$H = H_0 + H_1 \quad (5a)$$

dx.doi.org/10.1021/jp310177e | J. Phys. Chem. A 2013, 117, 594−606

$$H_0 = V_0 + \sum_{i=1}^{3} g_i(B_i^\dagger + B_i) + \sum_{i=1}^{3} \hbar\omega_i B_i^\dagger B_i - \frac{1}{2}\sum_{ij\neq 1}^{3} \gamma_{ij}(B_i^\dagger - B_i)(B_j^\dagger - B_j) + \frac{1}{2}\sum_{ij\neq 1}^{3} \varphi_{ij}(B_i^\dagger + B_i)(B_j^\dagger + B_j) + \frac{1}{3!}\sum_{ijk=1}^{3} g_{ijk}(B_i^\dagger + B_i)(B_j^\dagger + B_j)(B_k^\dagger + B_k) + \frac{1}{4!}\sum_{ijkl=1}^{3} g_{ijkl}(B_i^\dagger + B_i)(B_j^\dagger + B_j)(B_k^\dagger + B_k)(B_l^\dagger + B_l) + \frac{1}{5!}\sum_{ijklm=1}^{3} g_{ijklm}(B_i^\dagger + B_i)(B_j^\dagger + B_j)(B_k^\dagger + B_k)(B_l^\dagger + B_l)(B_m^\dagger + B_m) + \frac{1}{6!}\sum_{ijklmn=1}^{3} g_{ijklmn}(B_i^\dagger + B_i)(B_j^\dagger + B_j)(B_k^\dagger + B_k)(B_l^\dagger + B_l)(B_m^\dagger + B_m)(B_n^\dagger + B_n) \quad (5b)$$

$$H_1 = V_1 + g_4(B_4^\dagger + B_4) + \hbar\omega_4 B_4^\dagger B_4 - \frac{1}{2}\sum_{i=1}^{3} \gamma_{i4}(B_i^\dagger - B_i)(B_4^\dagger - B_4) + \frac{1}{2}\sum_{i=1}^{3} \varphi_{i4}(B_i^\dagger + B_i)(B_4^\dagger + B_4) - \frac{1}{3!}\sum_{i=1}^{3} \gamma'_{i44}(B_i^\dagger - B_i)(B_4^\dagger - B_4)(B_4^\dagger + B_4) - \frac{1}{3!}\sum_{i=1}^{3} \gamma''_{i44}(B_i^\dagger + B_i)(B_4^\dagger - B_4)(B_4^\dagger - B_4) + \frac{1}{3!}\sum_{i=1}^{4} g_{i44}(B_i^\dagger + B_i)(B_4^\dagger + B_4)(B_4^\dagger + B_4) + \frac{1}{4!}g_{4444}(B_4^\dagger + B_4)^4 + \frac{1}{5!}g_{44444}(B_4^\dagger + B_4)^5 + \frac{1}{6!}g_{44444}(B_4^\dagger + B_4)^6 \quad (5c)$$

where the dimensionless force constants are related to those in eq 1 by

$$g^{(n)}_{k1k2\cdots kn} = \sqrt{\frac{\hbar^n G_{k1k1}G_{k2k2}\cdots G_{knkn}}{2\omega_{k1}2\omega_{k2}\cdots 2\omega_{kn}}} f^{(n)}_{k1k2\cdots kn}$$

The bilinear ("mechanical") coupling includes both a kinetic (γ'_{ij}) and potential energy (φ_{ij}) contributions[46,52]

$$\gamma_{ij} = \gamma'_{ij} - \varphi_{ij} = -\frac{\sqrt{\omega_i\omega_j}\,G_{ij}}{2\sqrt{G_{ii}G_{jj}}} - \frac{\sqrt{\omega_i\omega_j}\,f_{ij}}{2\sqrt{f_{ii}f_{jj}}} \quad (6)$$

where γ'_{ij} is the kinetic energy contribution, and φ_{ij} is the potential energy contribution. In eq 5c, there are three terms which contribute to the Fermi resonance between the NH_2 bend and the N−H stretching coordinates. As in the bilinear coupling, there are both kinetic and potential energy contributions. The kinetic energy contributions are

$$\gamma'_{i44} = \left(\frac{\hbar}{2}\right)^{3/2}\sqrt{\frac{\omega_i}{G_{ii}}}\left(\frac{\partial G_{i4}}{\partial r_4}\right) \quad (7a)$$

$$\gamma''_{i44} = \left(\frac{\hbar}{2}\right)^{3/2}\sqrt{\frac{\omega_4^2 G_{ii}}{G_{44}^2\omega_i}}\left(\frac{\partial G_{44}}{\partial r_i}\right) \quad (7b)$$

The vibrational eigenstates were obtained by diagonalizing the Hamiltonian eq 5 in a harmonic basis, which was truncated at 12 quanta (1820 basis states). The anharmonic expansion coefficients, that are dominated by diagonal contributions, can be found in Table S3, Supporting Information.

The fundamental frequencies and anharmonicities for all four complexes are listed in Table 1. All frequencies and anharmonicities are scaled by a factor of 0.9183. This factor, which is larger than the standard harmonic scaling factor[53] and less than the recently determined anharmonic scaling factor, based on second-order vibrational perturbation theory calculations,[54,55] was chosen to match with experiment as in our previous study.[41] This scaling factor accurately reproduces the absolute position of the peaks as well as the splitting between the peaks.

Table 1. Calculated Fundamental Frequencies (ν_i), Anharmonicities (Δ_{ij}), and Local Anharmonicities (Δ_i^{loc}) in cm^{-1}, Calculated by Eqs 5a, 5b, and 5c

	WC	rWC	H	rH
ν_1	3063.65	3065.58	3069.36	3069.11
ν_2	3319.07	3324.21	3339.91	3344.07
ν_3	3476.61	3477.58	3477.88	3479.20
ν_4	1607.75	1608.14	1601.34	1601.59
$\Delta_{1,1}$	211.15	211.99	209.80	205.06
$\Delta_{2,2}$	72.32	74.97	81.74	81.76
$\Delta_{3,3}$	77.11	75.20	66.88	66.46
$\Delta_{4,4}$	30.68	30.04	25.07	24.67
$\Delta_{1,2}$	6.13	5.00	3.51	3.24
$\Delta_{1,3}$	0.94	0.97	1.01	0.96
$\Delta_{2,3}$	47.45	50.25	60.13	64.45
$\Delta_{1,4(2)}$	2.73	2.35	1.06	0.83
$\Delta_{2,4(2)}$	48.06	46.59	31.70	29.87
$\Delta_{2,4(2)}$	59.80	60.59	66.19	66.61
$\Delta^{loc}{}_1$	210.55	211.41	208.90	203.89
$\Delta^{loc}{}_2$	129.49	131.49	126.05	124.77
$\Delta^{loc}{}_3$	106.84	106.88	104.44	107.50
$\Delta^{loc}{}_4$	5.81	8.02	3.44	3.77

Due to the hydrogen bond formed by the NH_2 group of adenine in all four complexes, the NH_2 stretching modes are much more localized than in the 9-mA monomer. In the 9-mA monomer, the fundamental symmetric and antisymmetric NH_2 stretching modes contained a 50% contribution from each of the two local N−H modes. In the A·T base pairs, however, the symmetric NH_2 stretch is dominated by the hydrogen bonded N−H group of adenine (86%), and the antisymmetric stretch by the free N−H group of adenine (87%). The difference in the local mode frequencies caused by hydrogen bonding leads to an effective decoupling of the two local N−H oscillators on the NH_2 group, i.e., much less mixing of the N−H stretching normal modes.

dx.doi.org/10.1021/jp310177e | J. Phys. Chem. A 2013, 117, 594−606

The magnitude of the red shift in the N−H stretching frequencies is a clear indicator of the hydrogen bond strength. Our calculations show that in all four A·T complexes (see Figure 3a), the thymine N−H stretching mode has the lowest frequency, followed with increasing frequency by the hydrogen-bonded adenine N−H stretching mode, and the free adenine N−H stretching mode. Therefore, the thymine N−H hydrogen bond is stronger than the adenine N−H hydrogen bond. The fundamental frequencies for the thymine N−H stretching mode and the free N−H stretching mode of adenine are similar for all four complexes. In contrast, the hydrogen bonded N−H stretching mode of adenine shows a 25 cm^{-1} higher frequency in the Hoogsteen-type than in the Watson−Crick type complexes. This points to a slightly stronger hydrogen bond between the thymine C═O and the adenine N−H group in the Watson−Crick geometry. This difference is too small for resolving in the experimental spectra, because of the substantial broadening of the hydrogen-bonded N−H stretching absorption bands. For all four complexes, the NH_2 bending overtone frequency lies between the thymine N−H and the hydrogen-bonded adenine N−H stretching modes.

The local mode anharmonicities, which are obtained by expanding the Hamiltonian (eq 5) in one dimension and solving for the corresponding eigenstates, have also been calculated (Table 1). For weak hydrogen bonded systems, it is expected that the local anharmonicity will increase with the strength of the hydrogen bond.[56] While the local mode anharmonicity cannot be directly observed due to the inherent coupling between different oscillators, it provides an additional metric of the hydrogen bond strength. For all four complexes, the local mode anharmonicity is largest for the thymine N−H stretching mode, followed by the hydrogen-bonded adenine N−H stretching mode, and finally the free N−H stretching mode. The local anharmonicity of the free N−H stretching oscillator is roughly equal to the local anharmonicity of the N−H oscillators in 9-methyladenine monomer,[41] confirming the absence of a hydrogen bond for this N−H stretching transition.

The diagonal anharmonicities shed light on the relative hydrogen bond strengths of the N−H stretching oscillators and also the coupling between the different local modes (Table 1). The thymine N−H stretching local mode anharmonicity is equal to the thymine N−H stretching diagonal anharmonicity, which suggests that the thymine N−H stretching is uncoupled from the adenine N−H stretching oscillators. Interestingly, the diagonal anharmonicity of the adenine hydrogen-bonded N−H stretching oscillator is surprisingly small when compared to the free N−H stretching mode diagonal anharmonicity and the local mode anharmonicities for the adenine N−H stretching oscillators. We believe this surprisingly small anharmonicity is caused by the Fermi resonance of the hydrogen-bonded adenine N−H stretching oscillator with the adenine NH_2 bending.

To examine the effect of the Fermi resonance with the NH_2 bending on the diagonal anharmonicities of the adenine hydrogen-bonded N−H and free N−H stretching oscillators, we compared the fundamental frequencies and anharmonicities calculated with $H = H_0$ (i.e., excluding Fermi resonance contributions) and $H = H_0 + H_1$ (i.e., including Fermi resonance contributions). When the Fermi resonance with the NH_2 bending is excluded, the diagonal anharmonicity of the adenine N−H stretching mode is significantly larger than that of the free N−H stretching mode (Table 2). Therefore, the surprisingly small value of the adenine N−H stretching

Table 2. Calculated Fundamental Frequencies ($\nu_i^{(0)}$) and Diagonal Anharmonicities ($\Delta_{ij}^{(0)}$) Calculated Using Eq 5b

	WC	rWC	H	rH
$\nu_1^{(0)}$	3063	3065	3069	3069
$\nu_2^{(0)}$	3311	3317	3335	3335
$\nu_3^{(0)}$	3496	3498	3499	3499
$\Delta_{1,1}^{(0)}$	208	207	211	212
$\Delta_{2,2}^{(0)}$	114	111	103	102
$\Delta_{3,3}^{(0)}$	74	74	68	66

diagonal anharmonicity is caused by the Fermi resonance with the NH_2 bending mode. The decrease of the diagonal anharmonicity is caused by the coupling of the NH_2 bending $\delta = 2$ level and the adenine $\nu = 1$ level (leading to an increase of energy of the adenine N−H $\nu = 1$ level) as well as the coupling of the adenine N−H stretching $\nu = 2$ level and the combination level defined by the adenine N−H stretching $\nu = 1$ and the NH_2 bending $\delta = 2$ level (leading to a decrease of energy of the adenine N−H stretching $\nu = 2$ level).

The predicted stick spectra of the three fundamental N−H stretching transitions along with the NH_2 bending overtone transition are shown in Figure 3. The strength of the thymine N−H hydrogen bond causes the enhanced strength of this transition in all complexes.[57] This transition is the strongest, followed by the adenine hydrogen-bonded N−H stretching, the free N−H stretching, and the NH_2 bending overtone transitions. The NH_2 bending overtone transition has an oscillator strength which is roughly half that of the free N−H stretching transition. As the NH_2 bending overtone transition is strictly forbidden in the harmonic approximation, the oscillator strength of this transition must be caused by an anharmonic effect. The small diagonal anharmonicity of the NH_2 bending mode suggests that it is caused by a Fermi resonance with one of the N−H stretching modes.

The angles between the transition dipoles and the N−H bond vectors are shown in Figure 4 and Table 3. We note that for all N−H stretching fundamentals, the transition dipoles are largely oriented along their respective N−H bond vectors, due to the effective decoupling of the two local N−H stretching

Table 3. Angles between Eigenstate Transition Dipoles and N−H Bond Vectors in Degrees[a]

	WC	rWC	H	rH
$\angle(\mu_1,\mu_2)$	172.3	170.6	177.1	178.9
$\angle(\mu_1,\mu_3)$	33.0	31.9	49.2	48.3
$\angle(\mu_1,\mu_{4(1)})$	96.9	97.4	147.0	146.1
$\angle(\mu_1,\mu_{4(2)})$	169.4	167.7	178.7	177.1
$\angle(\mu_2,\mu_3)$	139.3	138.6	133.7	132.8
$\angle(\mu_2,\mu_{4(1)})$	75.4	73.2	35.9	35.1
$\angle(\mu_2,\mu_{4(2)})$	2.9	2.9	4.1	4.0
$\angle(\mu_3,\mu_{4(1)})$	63.9	65.5	82.2	82.2
$\angle(\mu_3,\mu_{4(2)})$	136.4	135.8	129.6	128.8
$\angle(\mu_{4(1)},\mu_{4(2)})$	72.5	70.3	31.7	31.0
$\angle(r_1,\mu_1)$	3.4	2.9	0.5	0.1
$\angle(r_2,\mu_2)$	2.2	3.7	17.5	19.0
$\angle(r_3,\mu_3)$	21.4	22.2	31.8	32.4
$\angle(r_2,\mu_{4(1)})$	77.5	76.9	53.4	54.1
$\angle(r_2,\mu_{4(2)})$	5.1	3.7	21.7	23.1

[a]The thymine N−H, adenine hydrogen-bonded N−H, and free N−H bond vectors are represented by r_1, r_2, and r_3, respectively. The transition dipoles μ_i (i = 1, 2, 3, 4(1), 4(2)) are labeled in Figure 4.

dx.doi.org/10.1021/jp310177e | J. Phys. Chem. A 2013, 117, 594−606

oscillators on the NH_2 group. For all four complexes, the NH_2 bending fundamental transition dipole points along the midpoint of the two adenine N−H bond vectors. However, the NH_2 bending overtone transition dipole is nearly parallel to the hydrogen-bonded adenine N−H stretching fundamental transition dipole. Therefore, the intensity of the NH_2 bending overtone transition is caused by a strong Fermi resonance of the NH_2 bending $\delta = 2$ state with the hydrogen-bonded adenine N−H stretching $\nu = 1$ state.

The Watson−Crick type complexes and the Hoogsteen-type complexes display few significant differences in the orientation of the transition dipoles (Table 3, Figure 4). First, the angle between the free N−H bond vector and the free N−H transition dipole is larger by ∼10° in the Hoogsteen-type conformations than in the WC-type conformations. Second, the NH_2 bending fundamental transition dipole is oriented at ∼53° to the adenine hydrogen-bonded N−H stretching transition dipole, while it is oriented at ∼75° in the WC-type conformations.

Summarizing the results of the ab initio calculations, each of the four different A·T complexes is predicted to show 3 N−H stretching fundamental bands and 1 NH_2 bending overtone band at distinct, but similar, frequency positions. The strength of the NH_2 bending overtone arises due to the strong Fermi resonance of the NH_2 bending overtone with the hydrogen-bonded adenine N−H stretching fundamental state. Adding up the contributions of all complexes, the predicted IR spectrum should display four major bands, as the differences in frequency positions of the four different complexes are clearly within the line width of the transitions observed in the linear IR spectra.

The theoretical predictions are in contrast to the spectra in Figure 3a which indicate at least six distinct spectral features associated with A·T complexes. The narrow band at 3482 cm^{-1} is associated with the free N−H group for all A·T base pair geometries, in line with the calculations and previous findings for G·C base pairs.[21] The spectral features with maxima at 3188, 3211, 3262, and 3324 cm^{-1} and, potentially, the broad wing extending from 2500 to 3000 cm^{-1} are all related to N−H stretching transitions of hydrogen-bonded N−H groups within the A·T base pairs for which theory predicts just four major bands. We conclude from this discrepancy that the line shapes in the experimental spectra are much more complex than just consisting of a single-peaked absorption band for each hydrogen-bonded N−H stretching mode and a single band for the NH_2 bending overtone. This conclusion is supported by the spectra of the partially deuterated A·T complexes (Figure 3b) which shows distinctly different line shapes and spectral widths of its components. In particular, the broad band between 2000 and 2300 cm^{-1} displays several maxima and a pronounced low-frequency tail. It should be noted that significantly broadened and structured N−H stretching line shapes have also been observed for systems such as the 7-azaindole dimer, where Fermi resonances of the N−H stretching mode with combination and overtones of fingerprint vibrations result in a distribution of the N−H stretching transition over a multitude of absorption lines.[16,17]

It is evident from this discussion that an interpretation and/or assignment of the different spectral features in the linear IR spectra requires additional independent information. Therefore, we apply femtosecond infrared pump−probe methods and 2D-IR spectroscopy to gain further insight into the spectral pattern and the couplings underlying the IR line shapes.

5. ULTRAFAST IR-PUMP−PROBE STUDIES AND 2D-IR SPECTRA

Spectrally and temporally resolved pump−probe data recorded with pump pulses centered at 3350 cm^{-1} are summarized in Figure 5b−d. In Figure 5b, the absorbance change $\Delta A = -^{10}\log(T/T_0)$ (T, T_0: sample transmission with and without excitation, respectively) is plotted as a function of probe frequency for different fixed delay times from 100 to 1000 fs. A pronounced decrease of absorption ($\Delta A < 0$) is observed at the frequency positions of the major components of the linear absorption spectrum. The negative ΔA is caused by the pump-induced depletion of the $\nu = 0$ ground state and stimulated emission from the $\nu = 1$ state of the underlying oscillators. The overall spectral envelopes are highly congested as they represent a superposition of the absorption decrease on the $\nu = 0$ to 1 transitions ($\Delta A < 0$) and an absorption increase on the $\nu = 1$ to 2 transitions ($\Delta A > 0$), the latter being indiscernible in the transient spectra. For at least a partial separation of such two components, the measurement of 2D vibrational spectra is mandatory.

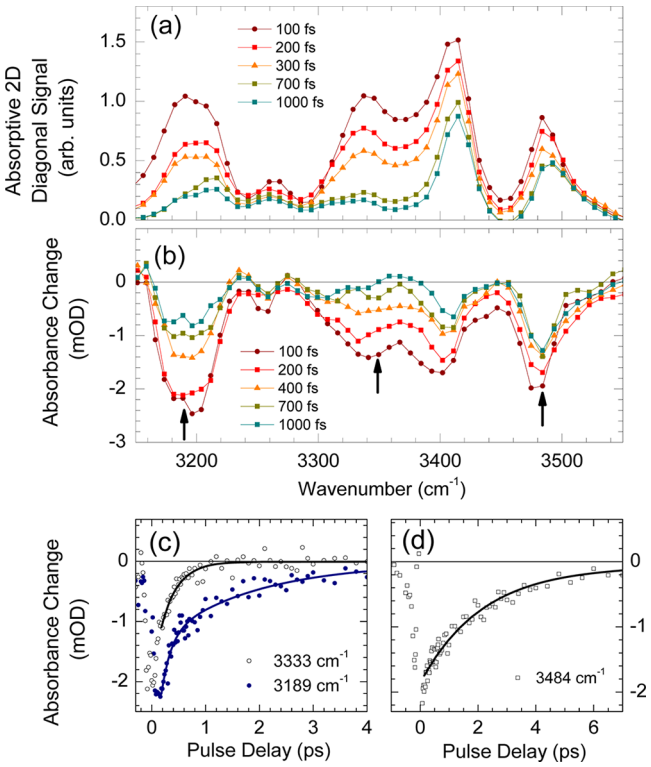

Figure 5. (a) Diagonal cuts of the 2D-IR spectra of 120 mM A·T in $CHCl_3$ as a function of the population waiting time T are compared with (b) transient IR-pump-IR-probe spectra. (c) Population kinetics of the bleach signals of N−H stretching bands associated with hydrogen-bonded N−H modes, as obtained at frequencies as indicated by the arrows in panel (b), can be compared with (d) population kinetics of the free N−H stretching modes located at 3484 cm^{-1}.

The spectral positions of the different bleaching contributions ($\Delta A < 0$) undergo minor changes as a function of pump−probe delay, pointing to a minor role of spectral diffusion beyond the spectral width of the respective components. The time-resolved traces taken at fixed probe frequencies (Figure 5d,e) demonstrate a bleach recovery on significantly faster time scales for the hydrogen-bonded N−H stretching components

dx.doi.org/10.1021/jp310177e | J. Phys. Chem. A 2013, 117, 594−606

than for the N−H stretching bands of A or T monomer, in accordance to previous reports on hydrogen-bonded N−H stretching modes.[17,20,21,41] Whereas the N−H symmetric stretching mode of the A monomers at 3415 cm^{-1}, as well as the 3484 cm^{-1} band associated with the free N−H stretching mode of A·T complexes, show population kinetics dominated by components with time constants ranging from 0.8 to 2.1 ps, the bands associated with A·T complexes located at 3200 and 3337 cm^{-1} show components with faster dynamics (see Table 4). This points to the faster depopulation of the underlying ν = 1 states which, at such lower energies, are in the range of anharmonically coupled overtone- and combination states of fingerprint modes, opening up additional pathways for population relaxation. It should be noted, however, that the time-dependent behavior for hydrogen-bonded N−H stretching excitations requires multiple exponential decay fitting functions. This indicates that the vibrational dynamics of the N−H stretching manifold on (sub)picosecond time scales follows vibrational energy flow pathways beyond a simple population decay mechanism for the different N−H stretching modes, consistent with what has been observed before for other hydrogen-bonded systems.[21,58−60]

Table 4. Relaxation Times of Different Vibrations Extracted from 2D-IR Photon Echo and Pump−Probe Measurements by Numerical Analysis

$\nu(0-1)$ (cm^{-1})	lifetime (ps)	type of measurement
3200	0.4 ± 0.1	2D diag. peak
	fast component: 0.18 ± 0.04	pump−probe
	slow component: 1.8 ± 0.2	
3337	0.46 ± 0.06	2D diag. peak
	0.31 ± 0.05	pump−probe
3415	0.8 ± 0.1	2D diag. peak
3484	1.1 ± 0.4	2D diag. peak
3484, average	2.1 ± 0.2	pump−probe
	1.8 ± 0.3	pump−probe
cross peak (ν_1, ν_3) (cm^{-1}, cm^{-1})	lifetime (ps)	type of measurement
(3484, 3389)	2 ± 1	2D off-diag. peak
(3409, 3329)	1.0 ± 0.4	2D off-diag. peak
(3393, 3251)	0.6 ± 0.1	2D off-diag. peak

To get insight into the origin of the absorption wing occurring between 2500 and 3000 cm^{-1} in the linear IR spectra (Figure 3a), we performed pump−probe experiments with pump pulses tuned to 2600 cm^{-1}. The transient spectra in Figure 6a show a bleach signal between 2500 and 2800 cm^{-1} that appears within the temporal resolution and displays a subsequent decay with temporal components <200 fs and 0.8 ± 0.1 ps (Figure 6c). In parallel, excitation at 2600 cm^{-1} causes a broadband bleaching on all N−H stretching components in the 3100−3600 cm^{-1} frequency range that originate from A·T complexes (Figure 6b). This absorption decrease which appears at delay zero and decays for the 3194 cm^{-1} band with temporal components of <200 fs and a 3.0 ± 0.9 ps time, mimics − within the experimental accuracy − the A·T related components of the steady-state IR spectrum in frequency position and band intensities. The <200 fs component is clearly obscured by the cross phase modulation signals around zero delay and can only be identified tentatively. No significantly strong bleach signals were found at frequency positions of free N−H stretching transitions of the A and T monomers. These important findings clearly show that the broad wing extending between 2500 and 3000 cm^{-1} is part of the overall line shape of N−H stretching absorption of the A·T complexes with its other components in the 3100−3500 cm^{-1} frequency range.

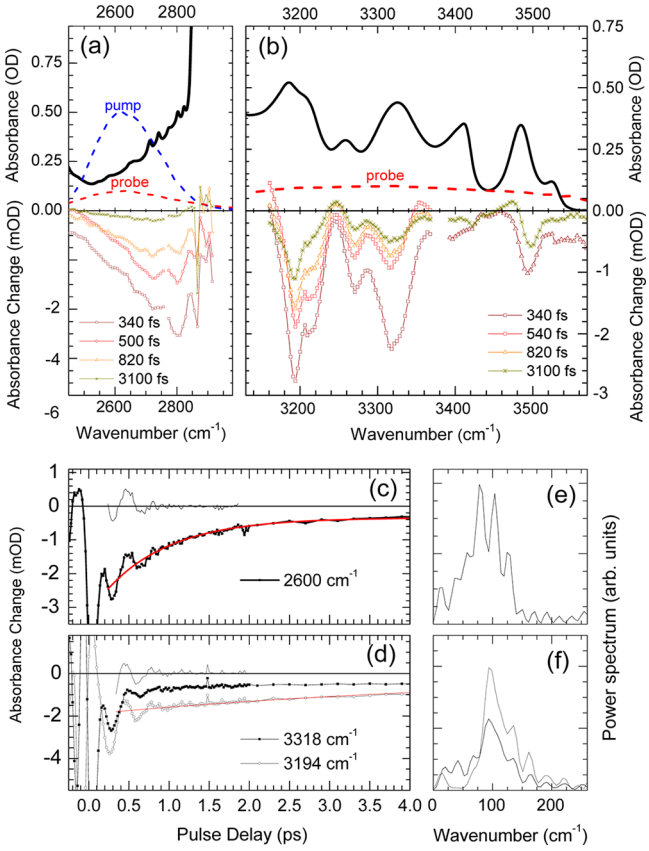

Figure 6. (a,b) Two-color IR-pump-IR-probe results measured on 120 mM A·T in $CHCl_3$, showing the transient response in the 2500−2800 cm^{-1} and the 3150−3600 cm^{-1} frequency ranges upon excitation at 2600 cm^{-1}. (c,d) The pump−probe transients show bleach recovery on a picosecond time scale. The oscillatory signal in these pump−probe transients, obtained after subtraction of the population kinetics components, is ascribed to a coherent wavepacket motion of an underdamped mode, with a frequency spectrum as shown in panels (e,f).

The time-resolved data taken with pumping at 2600 cm^{-1} (Figure 6c,d) and probing either below or above the C−H stretching region exhibit an oscillatory component whereof the Fourier transform is centered around 100 cm^{-1} (Figure 6e,f). The oscillations are due to coherent wavepacket motions in a low-frequency mode that couples anharmonically to the N−H stretching vibration. Broadband excitation of the N−H stretching vibration by a sub-100 fs pump pulse generates a quantum-coherent superposition of levels of this low-frequency mode which propagates in time and modulates the N−H stretching absorption. This modulation is read out by the probe pulses monitoring changes of N−H stretching absorption. The frequency of 100 cm^{-1} is in a typical range for hydrogen bond modes, in particular stretching modes modulating the length of the two hydrogen bonds in the A·T complexes. A similar behavior has been observed in a number of hydrogen-bonded dimer systems, e.g., acetic acid dimer,[12−15] 7-azaindole dimer,[16,17] and 2-pyridone dimer.[18,19]

For a more detailed insight into the complex N−H stretching coupling scheme and line shapes, we performed IR photon echo measurements of A·T complexes to derive 2D IR spectra.

dx.doi.org/10.1021/jp310177e | J. Phys. Chem. A 2013, 117, 594−606

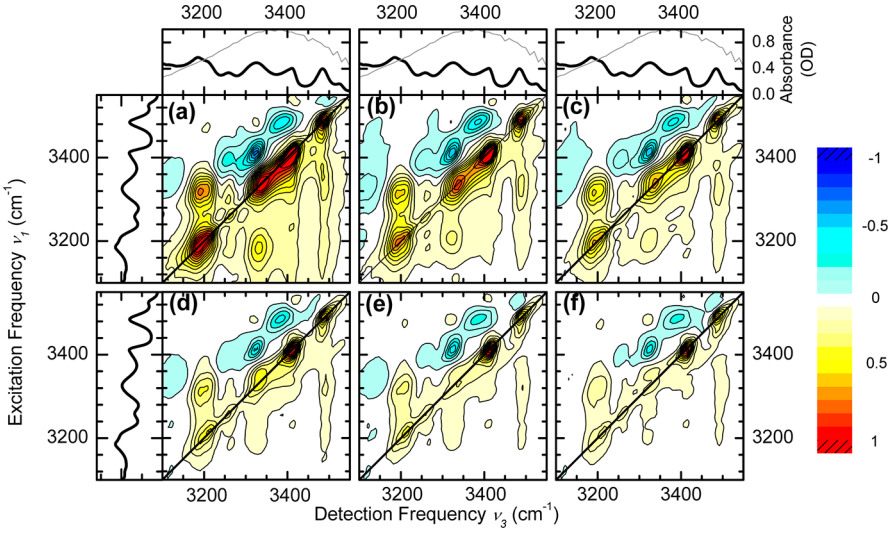

Figure 7. Absorptive 2D-IR spectra of A·T measured in $CHCl_3$, measured for the *ZZZZ* polarization configuration of excitation and local oscillator pulses, as function of waiting time *T*: (a) 100 fs, (b) 200 fs, (c) 300 fs, (d) 500 fs, (e) 700 fs, and (f) 1000 fs. The intensity of the peaks in these 2D-IR spectra are rescaled to 60% of the maximum signal in the *T* = 100 fs 2D spectra. For comparison the linear IR spectra and the laser spectrum have been added to this graph.

In the case of dissimilar N−H stretching behavior for WC/rWC and H/rH A·T complexes the absence of particular cross peaks of N−H stretching transitions of A·T complexes is expected, whereas for a similar behavior the connection between the N−H stretching transitions in the 2D-IR spectra should be evidenced by a full presence of all possible cross peaks. In Figure 7, we present the 2D-IR spectra of the A·T complexes as a function of waiting time *T*. In these measurements we used the parallel $(\boldsymbol{k}_1,\boldsymbol{k}_2,\boldsymbol{k}_3,\boldsymbol{k}_{LO})$ = (*ZZZZ*) polarization geometry for all four beams. The 2D spectra show diagonal peaks at $(\nu_1[\text{cm}^{-1}], \nu_3[\text{cm}^{-1}])$ = (3200, 3200), (3263, 3263), (3337, 3337), (3415, 3415), and (3484, 3484) and a shoulder at (3525, 3525), in full accordance with transitions observed in the linear FT-IR spectra (Figures 2 and 3). For comparison we show cuts of the 2D-IR spectra along the diagonal in Figure 5a, in accordance with both the linear FT-IR and the nonlinear IR-pump−probe spectra. The peak line shapes do not notably change as a function of population time within our experimental resolution hinting at only little structural fluctuations in the A·T dimer geometries up to 1 ps, as already indicated by their transient absorption behavior. Off-diagonal peaks at (3200, 3320), (3320, 3200), (3200, 3484), (3484, 3200), (3320, 3484), and (3484, 3320) and a minor cross peak at (3525, 3420) are also clearly present. Off-diagonal peaks with opposite sign are observed at (3484, 3389), (3409, 3329), and (3393, 3251). These can be assigned as $\nu = 1 \rightarrow \nu = 2$ excited state pathway contributions connected to the fundamental $\nu = 0 \rightarrow \nu = 1$ fundamental transitions of the A·T complexes at 3484 cm^{-1}, the 3409 cm^{-1} transition of the A monomer, and the 3393 cm^{-1} transition of the T monomer, respectively. Interestingly, the (3320, 3200) cross peak clearly shows a relative intensity increase compared to the (3320, 3320) diagonal peak with increasing population waiting time *T*. In contrast, no such behavior is apparent for the ratio of the (3200, 3320) cross peak and the (3200, 3200) diagonal peak. This suggests an ultrafast downhill vibrational energy transfer on a picosecond time scale as was similarly reported for G·C base pairs[21] and A·T oligomer films.[60] For all other peaks, the cross-to-diagonal peak ratio does not show notable changes in time.

Figure 8 shows a comparison of the 2D-IR spectra measured for polarization conditions of $(\boldsymbol{k}_1,\boldsymbol{k}_2,\boldsymbol{k}_3,\boldsymbol{k}_{LO})$ equal to (*ZZZZ*) or

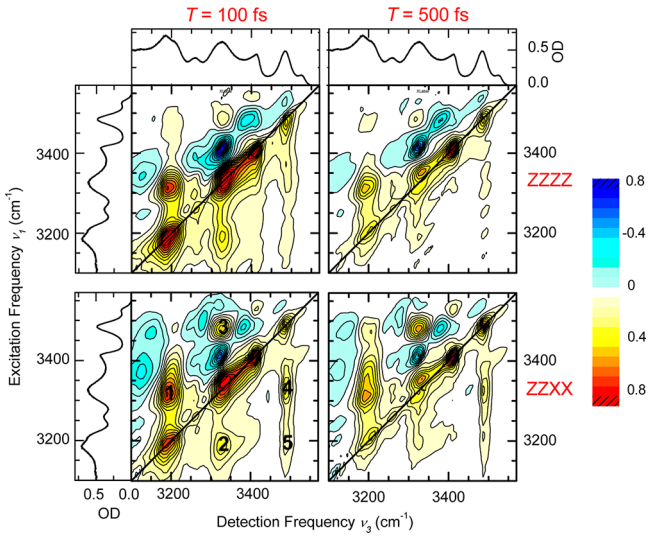

Figure 8. Absorptive 2D-IR spectra of 140 mM A·T measured in $CHCl_3$, measured for the *ZZZZ* and *ZZXX* polarization configurations of excitation and local oscillator pulses, as function of waiting time *T*. For clarity purposes the intensity of these 2D-IR spectra have been rescaled to 80% of the maximum value. For comparison the solvent corrected linear IR spectra have been added to this graph. The cross peaks, as analyzed with eq 8, have been indexed in the lower left 2D-IR spectrum.

(*ZZXX*). In the latter case the strength of the diagonal peaks diminishes.[61] The intensities of the cross peaks located at (3320, 3484) and (3484, 3320) have become larger relative to the diagonal peaks. This is also the case for the (3525, 3420) and (3420, 3525), the (3200, 3484), and to a lesser extent (3484, 3200) cross peaks. In contrast, the (3200, 3320) and (3320, 3200) cross peak intensities do not change compared to

dx.doi.org/10.1021/jp310177e | J. Phys. Chem. A 2013, 117, 594−606

the (3200, 3200) and (3320, 3320) diagonal peaks when altering the polarization geometry. Additional contributions with negative sign, connected to the positive cross peaks, also become visible when using the perpendicular (*ZZXX*) polarization geometry, see e.g. the peaks at (3307, 3449), (3482, 3277), and (3482, 3155).

The (3525, 3420) and (3420, 3525) positive cross peaks are indicative of coupling between the two N−H stretching local modes of A monomer, as has been shown in a recent 2D study of the adenosine monomer.[41] The 2D spectra in Figures 7 and 8 demonstrate that all N−H stretching components associated with A·T complexes exhibit positive cross peaks. This is true not only for the N−H stretching transition associated with the free non-hydrogen-bonded NH group located at 3484 cm^{-1}, showing cross peaks with the 3200 and 3320 cm^{-1} transitions, but also for the components originating from the hydrogen bonded N−H stretching oscillators.

The single spectral N−H stretching feature at 3484 cm^{-1} can safely be assigned to the free N−H unit of the NH_2 group of adenosine, as supported by the theoretical calculations of section 3. This mode displays cross peaks with all other N−H stretching features of the A·T complexes, due to its pronounced coupling to the stretching modes of the hydrogen bonded N−H groups. The latter gives rise to a multitude of strongly coupled spectral features at lower frequencies, including the low-frequency wing below the C−H stretching bands, a fact that is evident from both the pump−probe and the 2D data. This breakup into a multitude of lines is mainly caused by Fermi resonances of the N−H stretching modes with combination and overtones of fingerprint vibrations, the dipole-allowed $v = 0 \rightarrow v = 1$ N−H stretching transitions providing the oscillator strength to the dipole forbidden combination or overtone transitions. In principle, polarization resolved 2D spectra such as shown in Figure 8 can assist in identifying such a particular subset of coupled transitions, because then the diagonal and off-diagonal peaks should undergo the same relative change of intensity when changing the polarization conditions.[62] Instead of directly comparing cross peak intensities recorded for different polarization geometries (C_{ZZZZ}, C_{ZZXX}), we divide the cross peak intensities by their corresponding diagonal peak intensities (D_{ZZZZ}, D_{ZZXX}) to correct for possible slow drifts of laser intensities or laser pointing during the measurements. For the absorptive 2D-IR spectra, the ratio $f_{\alpha\beta}$

$$f_{\alpha\beta} = \frac{C_{ZZXX}/D_{ZZXX}}{C_{ZZZZ}/D_{ZZZZ}} \tag{8a}$$

is related to the relative angle of transition dipole moments $\Theta_{\alpha\beta}$ of the vibrational transitions α and β that share the cross peak in the 2D-IR spectra (see Table 5), as defined by the formula

$$f_{\alpha\beta} = = \frac{10 - P_2(\Theta_{\alpha\beta})}{4P_2(\Theta_{\alpha\beta}) + 5} \tag{8b}$$

Table 5. Peak Intensity Ratio $f_{\alpha\beta}$ for the Cross Peaks Numbered in Figure 8 Measured under (*ZZZZ*) and (*ZZXX*) Polarization Configurations

peak	1	2	3	4	5
$f_{\alpha\beta}$	1.1 ± 0.4	1.1 ± 0.2	3.6 ± 1.3	2.5 ± 0.4	2.5 ± 0.3
$\Theta_{\alpha\beta}$	20 ± 20	20 ± 20	90 ± 30	65 ± 8	65 ± 8

with $P_2(\Theta_{\alpha\beta})$ the second order Legendre polynomial of $\Theta_{\alpha\beta}$. To judge whether population or coherence transfer would affect this parameter, we measured polarization-dependent 2D-IR spectra at different population times T (typically T = 100, 200, and 500 fs) and extrapolate the derived ratio $f_{\alpha\beta}$ to T = 0 fs. Comparing the obtained values for peaks 1 and 2 on one side, and those for peaks 3, 4, and 5 on the other side (for peak index see Figure 8), it follows that the transition dipole moments of the free N−H stretching vibration at 3384 cm^{-1} and the N−H stretching vibrations associated with hydrogen-bonded N−H motions at 3200 and 3320 cm^{-1} have a relative angle ranging from 65 to 90°, while the angle between the transition dipole moments of the 3200 and 3320 cm^{-1} transitions is about 20°. Taking into account the magnitude of the error margins of these derived values of relative angles of transition dipole moments, and realizing that the outcome of this analysis is an average of four different nucleobase pair geometries, it follows that the results are in accordance with the calculated results given in Table 3. The fact that a substantial Fermi coupling of the v = 1 N−H stretching levels of adenosine with the NH_2-bending δ = 2 overtone level exists not only has major repercussions in the apparent splitting of transitions at 3200 and 3320 cm^{-1} with large cross sections but also has consequences for the relative orientation of the transition dipole moments of the $v = 0 \rightarrow v = 1$ fundamental N−H stretching transitions of the hydrogen-bonded and free NH-groups compared to the bending fundamental and overtone transitions of the NH_2-group of adenosine within the A·T nucleobase pairs. While the $\delta = 0 \rightarrow \delta = 1$ bending fundamental has its transition dipole moment $\boldsymbol{\mu}_{4(1)}$ oriented 80° relative to the transition dipole moment $\boldsymbol{\mu}_2$ of the $v = 0 \rightarrow v = 1$ fundamental N−H stretching transition of the hydrogen-bonded NH, the transition dipole moment $\boldsymbol{\mu}_{4(2)}$ of its $\delta = 0 \rightarrow \delta = 2$ first overtone is almost parallel to it (see Figure 4). Such a large change in transition dipole moment direction can only result when extensive mixing of v = 1 stretching and δ = 2 bending states by Fermi resonance coupling takes place.

In closing this section we emphasize that the consistency in the dependence of intensity ratios between diagonal and cross peaks with polarization geometries of the ($\boldsymbol{k}_1$,$\boldsymbol{k}_2$,$\boldsymbol{k}_3$,$\boldsymbol{k}_{LO}$) laser beams fully follows the picture that all transitions associated with the A·T nucleobase pairs share a common vibrational ground state, i.e. no significant transitions of other species with a single particular peak contribute to the linear FT-IR and nonlinear 2D-IR spectra. Because structural fluctuations caused by the solvent leads to a N−H stretching transition frequency distribution following a smooth dependence,[63,64] a significant line broadening results without additional specific substructures due to these solvent fluctuations. As such we conclude that the linear and nonlinear N−H stretching spectra are governed by the four double hydrogen-bonded A·T nucleobase pairs as depicted in Figure 1, as well as the A and T monomers.

6. CONCLUSIONS

We have now come to the following picture of the nucleobase pairs of A and T. Our investigations clearly hint at the simultaneous existence of four different heterodimer complex species in chloroform solution. Quantum chemical calculations, two-color pump−probe data, and the evaluation of cross-peak-patterns in 2D-IR spectra show that their spectroscopic and structural properties are similar, with only small differences in hydrogen stretching frequency shifts, cross sections, and vibrational couplings. Structural information obtained from X-

dx.doi.org/10.1021/jp310177e | J. Phys. Chem. A 2013, 117, 594−606

ray and neutron diffraction on crystals of A·U and A·T complexes in Watson−Crick and Hoogsteen geometries[1,50,51] and NMR and quantum chemical calculations of A·T complexes in solution show that the N−H···N and N−H···O hydrogen bond distances range from 2.9−3.0 Å. The frequency position of the three N−D stretching bands of the N−D stretching manifold in deuterated A·T complexes can be connected to the N−H stretching bands by use of the empirical scaling factor of 1.35 for the H/D exchange isotope effect of hydrogen stretching oscillators.[10]

Nonetheless, a mode assignment of the N−H/N−D stretching manifold in a local mode picture containing only the hydrogen-bonded thymidine N−H stretching mode $\nu_T(N-H)_b/\nu_T(N-D)_b$, a hydrogen-bonded adenosine N−H stretching $\nu_A(N-H)_b/\nu_A(N-D)_b$, and a free adenosine N−H/N−D stretching mode $\nu_A(N-H)_f/\nu_A(N-D)_f$ is insufficient. Actually, the higher complexity in the N−H stretching manifold is caused by the fact that there are two N−H stretching oscillators per A·T complex involved in hydrogen bonding, providing oscillator strength and displaying a mutual coupling, on top of giving rise to a breakup of the spectral envelopes. In particular a Fermi resonance with the NH_2 bending mode of adenosine $(2\delta_A(NH_2)_b)$ leads to a pronounced change of the N−H stretching manifold. Only after inclusion of this Fermi resonance a satisfactory correspondence between experimental and theoretical spectra results. One should realize, however, that a substantial mixing between the calculated modes occurs, and a pure local mode picture no longer represents the correct description for the N−H stretching manifolds of the A·T complexes. As such a direct one-to-one correspondence between the $\nu_T(N-H)_b$, $\nu_A(N-H)_b$, $\nu_A(N-H)_f$, and $2\delta_A(NH_2)_b$ to particular bands is not appropriate anymore.

As a result, the concept of a mode description using local hydrogen-bonded N−H stretching oscillators of adenosine and thymidine is clearly not sufficient and has to be replaced by a picture of a coupled manifold of N−H stretching and fingerprint degree of freedoms. In contrast to vibrational assignments based on a one-to-one correspondence between spectral features in linear infrared spectra and particular N−H stretching modes,[6,23,65,66] the present nonlinear infrared study clearly shows the much more complex character of the infrared line shapes. Similar behavior is found for other model systems forming medium-strong hydrogen bonds with O−H stretching, such as in cyclic carboxylic acid dimers, or N−H stretching vibrations, such as in 7-azaindole dimers.[12−19] It calls for in-depth theoretical calculations of couplings and spectra that include a subset of fingerprint modes, among them the NH_2 bending mode and modes involving elongations of the acceptor atoms in the two hydrogen bonds of the A·T complexes. Such work, clearly beyond the scope of the present study, will be the next challenge in deciphering the spectroscopy of N−H stretching vibrations in nucleobase pairs. Model systems in which a particular nucleobase pairing geometry is enforced, e.g., double-stranded DNA oligomers, can provide independent additional insight.

■ ASSOCIATED CONTENT

Supporting Information

NMR experiments, temperature-dependent FT-IR spectra, full listing of ref 25, and results of ab initio calculations. This material is available free of charge via the Internet at http://pubs.acs.org.

■ AUTHOR INFORMATION

Corresponding Author

*E-Mail: nibberin@mbi-berlin.de.

Notes

The authors declare no competing financial interest.

■ ACKNOWLEDGMENTS

This research has received funding from the European Research Council under the European Union's Seventh Framework Programme (FP7/2007-2013)/ERC grant agreement no. 247051 (T.E.), the German Science Foundation (Deutsche Forschungsgemeinschaft, F.T.), the National Institutes of Health (Grants GM059230 and GM091364; S.M.), and the National Science Foundation (Grant CHE-1058791; S.M.). N.K.P. is supported by a National Science Foundation Graduate Research Fellowship.

■ REFERENCES

(1) Saenger, W. *Principles of Nucleic Acid Structure*; Springer: New York, 1984.

(2) *Oxford Handbook of Nucleic Acid Structure*; Neidle, S., Ed.; Oxford University Press: Oxford, U.K., 1999.

(3) Fonseca Guerra, C.; Bickelhaupt, F. M.; Snijders, J. G.; Baerends, E. J. *Chem.—Eur. J.* **1999**, *5*, 3581−3594.

(4) Fonseca Guerra, C.; Bickelhaupt, F. M.; Snijders, J. G.; Baerends, E. J. *J. Am. Chem. Soc.* **2000**, *122*, 4117−4128.

(5) Hobza, P.; Šponer, J. *Chem. Rev.* **1999**, *99*, 3247−3276.

(6) de Vries, M. S.; Hobza, P. *Annu. Rev. Phys. Chem.* **2007**, *58*, 585−612.

(7) Ribeiro, R. F.; Marenich, A. V.; Cramer, C. J.; Truhlar, D. G. *Phys. Chem. Chem. Phys.* **2011**, *13*, 10908−10922.

(8) Dunger, A.; Limbach, H.-H.; Weisz, K. *Chem.—Eur. J.* **1998**, *4*, 621−628.

(9) Dunger, A.; Limbach, H.-H.; Weisz, K. *J. Am. Chem. Soc.* **2000**, *122*, 10109−10114.

(10) Novak, A. *Struct. Bonding (Berlin, Ger.)* **1974**, *18*, 177−216.

(11) Lautié, A.; Froment, F.; Novak, A. *Spectrosc. Lett.* **1976**, *9*, 289−299.

(12) Heyne, K.; Huse, N.; Dreyer, J.; Nibbering, E. T. J.; Elsaesser, T.; Mukamel, S. *J. Chem. Phys.* **2004**, *121*, 902−913.

(13) Huse, N.; Bruner, B. D.; Cowan, M. L.; Dreyer, J.; Nibbering, E. T. J.; Miller, R. J. D.; Elsaesser, T. *Phys. Rev. Lett.* **2005**, *95*, 147402.

(14) Dreyer, J. *J. Chem. Phys.* **2005**, *122*, 184306.

(15) Dreyer, J. *Int. J. Quantum Chem.* **2005**, *104*, 782−793.

(16) Dreyer, J. *J. Chem. Phys.* **2007**, *127*, 054309.

(17) Dwyer, J. R.; Dreyer, J.; Nibbering, E. T. J.; Elsaesser, T. *Chem. Phys. Lett.* **2006**, *432*, 146−151.

(18) Szyc, Ł.; Guo, J.; Yang, M.; Dreyer, J.; Tolstoy, P. M.; Nibbering, E. T. J.; Czarnik-Matusewicz, B.; Elsaesser, T.; Limbach, H.-H. *J. Phys. Chem. A* **2010**, *114*, 7749−7760.

(19) Yang, M.; Szyc, Ł.; Dreyer, J.; Nibbering, E. T. J.; Elsaesser, T. *J. Phys. Chem. A* **2010**, *114*, 12195−12201.

(20) Woutersen, S.; Cristalli, G. *J. Chem. Phys.* **2004**, *121*, 5381−5386.

(21) Yang, M.; Szyc, Ł.; Rottger, K.; Fidder, H.; Nibbering, E. T. J.; Elsaesser, T.; Temps, F. *J. Phys. Chem. B* **2011**, *115*, 5484−5492.

(22) Nir, E.; Kleinermanns, K.; de Vries, M. S. *Nature* **2000**, *408*, 949−951.

(23) Abo-Riziq, A.; Grace, L.; Nir, E.; Kabelac, M.; Hobza, P.; de Vries, M. S. *Proc. Natl. Acad. Sci. U.S.A.* **2005**, *102*, 20−23.

(24) Schwalb, N. K.; Michalak, T.; Temps, F. *J. Phys. Chem. B* **2009**, *113*, 16365−16376.

(25) Frisch, M. J.; Trucks, G. W.; Schlegel, H. B.; Scuseria, G. E.; Robb, M. A.; Cheeseman, J. R.; Scalmani, G.; Barone, V.; Mennucci, B.; Petersson, G. A.; et al. *Gaussian 09*, Revision A.1; Gaussian, Inc.: Wallingford, CT, 2009.

(26) Barone, V.; Cossi, M. *J. Phys. Chem. A* **1998**, *102*, 1995−2001.

(27) Cossi, M.; Rega, N.; Scalmani, G.; Barone, V. *J. Comput. Chem.* **2003**, *24*, 669−681.
(28) Limbach, H.-H.; Tolstoy, P. M.; Pérez-Hernández, N.; Guo, J.; Shenderovich, I. G.; Denisov, G. S. *Isr. J. Chem.* **2009**, *49*, 199−216.
(29) Tolstoy, P. M.; Guo, J.; Koeppe, B.; Golubev, N. S.; Denisov, G. S.; Smirnov, S. N.; Limbach, H.-H. *J. Phys. Chem. A* **2010**, *114*, 10775−10782.
(30) Koeppe, B.; Tolstoy, P. M.; Limbach, H.-H. *J. Am. Chem. Soc.* **2011**, *133*, 7897−7908.
(31) Guo, J.; Tolstoy, P. M.; Koeppe, B.; Denisov, G. S.; Limbach, H.-H. *J. Phys. Chem. A* **2011**, *115*, 9828−9836.
(32) Weisz, K.; Jähnchen, J.; Limbach, H.-H. *J. Am. Chem. Soc.* **1997**, *119*, 6436−6437.
(33) Vakonakis, I.; LiWang, A. C. *J. Am. Chem. Soc.* **2004**, *126*, 5688−5689.
(34) Swart, M.; Fonseca Guerra, C.; Bickelhaupt, F. M. *J. Am. Chem. Soc.* **2004**, *126*, 16718−16719.
(35) Biemann, L.; Haber, T.; Kleinermanns, K. *J. Chem. Phys.* **2009**, *130*, 125102.
(36) Biemann, L.; Haber, T.; Maydt, D.; Schaper, K.; Kleinermanns, K. *J. Chem. Phys.* **2008**, *128*, 195103.
(37) Schwalb, N. K.; Temps, F. *J. Photochem. Photobiol., A* **2009**, *208*, 164−170.
(38) Biemann, L.; Haber, T.; Maydt, D.; Schaper, K.; Kleinermanns, K. *J. Chem. Phys.* **2011**, *134*, 115103.
(39) Hamlin, R. M., Jr.; Lord, R. C.; Rich, A. *Science* **1965**, *148*, 1734−1737.
(40) Miller, J. H.; Sobell, H. M. *J. Mol. Biol.* **1967**, *24*, 345−350.
(41) Greve, C.; Preketes, N. K.; Costard, R.; Koeppe, B.; Fidder, H.; Nibbering, E. T. J.; Temps, F.; Mukamel, S.; Elsaesser, T. *J. Phys. Chem. A* **2012**, *116*, 7636−7644.
(42) Schäfer, A.; Horn, H.; Ahlrichs, R. *J. Chem. Phys.* **1992**, *97*, 2571−2577.
(43) Halonen, L.; Carrington, T. *J. Chem. Phys.* **1988**, *88*, 4171−4185.
(44) Moran, A. M.; Dreyer, J.; Mukamel, S. *J. Chem. Phys.* **2003**, *118*, 1347−1355.
(45) Hayashi, T.; Mukamel, S. *J. Phys. Chem. A* **2003**, *107*, 9113−9131.
(46) Wilson, E. B.; Decius, J. C.; Cross, P. C. *Molecular Vibrations*; Dover Publications: New York, 1980.
(47) Bowman, J. M. *Acc. Chem. Res.* **1986**, *19*, 202−208.
(48) Ratner, M. A.; Gerber, R. B. *J. Phys. Chem.* **1986**, *90*, 20−30.
(49) Mills, I. M. In *Modern Spectroscopy: Modern Research*; Rao, K. N., Matthews, C. W., Eds.; Academic Press: New York, 1972; pp 115−140.
(50) Seeman, N. C.; Rosenberg, J. M.; Suddath, F. L.; Kim, J. J. P.; Rich, A. *J. Mol. Biol.* **1976**, *104*, 109−144.
(51) Frey, M. N.; Koetzle, T. F.; Lehmann, M. S.; Hamilton, W. C. *J. Chem. Phys.* **1973**, *59*, 915−924.
(52) Kjaergaard, H. G.; Garden, A. L.; Chaban, G. M.; Gerber, R. B.; Matthews, D. A.; Stanton, J. F. *J. Phys. Chem. A* **2008**, *112*, 4324−4335.
(53) Merrick, J. P.; Moran, D.; Radom, L. *J. Phys. Chem. A* **2007**, *111*, 11683−11700.
(54) Barone, V. *J. Chem. Phys.* **2005**, *122*, 014108.
(55) Johnson, R. D.; Irikura, K. K.; Kacker, R. N.; Kessel, R. *J. Chem. Theor. Comput.* **2010**, *6*, 2822−2828.
(56) Sándorfy, C. *J. Mol. Struct.* **2006**, *790*, 50−54.
(57) Wang, G. X.; Ma, X. Y.; Wang, J. P. *Chin. J. Chem. Phys.* **2009**, *22*, 563−570.
(58) Kozich, V.; Dreyer, J.; Ashihara, S.; Werncke, W.; Elsaesser, T. *J. Chem. Phys.* **2006**, *125*, 074504.
(59) Kozich, V.; Dreyer, J.; Werncke, W. *J. Chem. Phys.* **2009**, *130*, 034505.
(60) Yang, M.; Szyc, Ł.; Elsaesser, T. *J. Phys. Chem. B* **2011**, *115*, 1262−1267.
(61) Zanni, M. T.; Ge, N.-H.; Kim, Y. S.; Hochstrasser, R. M. *Proc. Natl. Acad. Sci. U.S.A.* **2001**, *98*, 11265−11270.
(62) Hamm, P.; Zanni, M. *Concepts and Methods of 2D Infrared Spectroscopy*; Cambridge University Press: Cambridge, 2011.
(63) Krishnan, G. M.; Kühn, O. *Chem. Phys. Lett.* **2007**, *435*, 132−135.
(64) Yan, Y. A.; Krishnan, G. M.; Kühn, O. *Chem. Phys. Lett.* **2008**, *464*, 230−234.
(65) Plützer, C.; Hünig, I.; Kleinermanns, K.; Nir, E.; de Vries, M. S. *ChemPhysChem* **2003**, *4*, 838−842.
(66) Brauer, B.; Gerber, R. B.; Kabeláč, M.; Hobza, P.; Bakker, J. M.; Abo Riziq, A. G.; de Vries, M. S. *J. Phys. Chem. A* **2005**, *109*, 6974−6984.

NOTE ADDED AFTER ASAP PUBLICATION

This article posted ASAP on January 7, 2013. Sentence 3 has been revised in the paragraph following equation 3. In the Conclusions section, a sentence has been deleted in the first paragraph. The correct version posted on January 15, 2013.